Femtosecond pump-probe spectroscopy of propagating coherent acoustic phonons in $In_xGa_{1-x}N/GaN$ heterostructures

Rongliang Liu, G. D. Sanders, and C. J. Stanton
Department of Physics, University of Florida, Box 118440, Gainesville, Florida 32611-8440, USA

Chang Sub Kim
Department of Physics, Chonnam National University, Kwangju 500-757, Korea

J. S. Yahng, Y. D. Jho, K. J. Yee, E. Oh, and D. S. Kim
Department of Physics, Seoul National University, Seoul 151-742, Korea

(Received 28 October 2003; revised manuscript received 2 September 2005; published 23 November 2005)

We show that large amplitude coherent acoustic phonon wave packets can be generated and detected in $In_xGa_{1-x}N/GaN$ epilayers and heterostructures in femtosecond pump-probe differential reflectivity experiments. The amplitude of the coherent phonon increases with increasing indium fraction x and unlike other coherent phonon oscillations, both *amplitude* and *period* are strong functions of the laser probe energy. The amplitude of the oscillation is substantially and almost instantaneously reduced when the wave packet reaches a GaN-sapphire interface below the surface indicating that the phonon wave packets are useful for imaging below the surface. A theoretical model is proposed which fits the experiments well and helps to deduce the strength of the phonon wave packets. Our model shows that localized coherent phonon wave packets are generated by the femtosecond pump laser in the epilayer near the surface. The wave packets then propagate through a GaN layer changing the local index of refraction and, as a result, modulate the reflectivity of the probe beam. Our model correctly predicts the experimental dependence on probe wavelength as well as epilayer thickness.

DOI: 10.1103/PhysRevB.72.195335 PACS number(s): 78.66.Fd, 78.47.+p, 78.20.Hp

I. INTRODUCTION

Heterostructures of GaN and InGaN are important materials owing to their applications to blue laser diodes and high-power electronics.[1] Strong coherent acoustic phonon oscillations have recently been detected in InGaN/GaN multiple quantum wells.[2,3] These phonon oscillations were much stronger than folded acoustic phonon oscillations observed in other semiconductor superlattices.[4–6]

InGaN/GaN heterostructures are highly strained at high In concentrations giving rise to large built-in piezoelectric fields,[7–10] and the large strength of the coherent acoustic phonon oscillations was attributed to the large strain and piezoelectric fields.[2]

In this paper, we report the generation of strong localized coherent phonon wave packets in strained layer $In_xGa_{1-x}N/GaN$ epilayers and heterostructures grown on GaN and sapphire substrates.[11] By focusing high repetition rate frequency-doubled femtosecond Ti:Sapphire laser pulses onto strongly strained InGaN/GaN heterostructures, we can, through the carrier-phonon interaction, generate coherent phonon wave packets which are initially localized near the epilayer/surface but then propagate away from the surface/epilayer and through a GaN layer. As the wave packets propagate, they modulate the local index of refraction and can be observed in the time-dependent differential reflectivity of the probe pulse. There is a sudden drop in the amplitude of the reflectivity oscillation of the probe pulse when the phonon wave packet reaches a GaN-sapphire interface below the surface. Theoretical calculations as well as experimental evidence support this picture; the sudden drop of amplitude when the wave encounters the GaN-sapphire interface cannot be explained if the wave packet had a large spatial extent. When the wave packet encounters the GaN-sapphire interface, part of the wave gets reflected while most of it gets transmitted into the sapphire substrate, depending on the interface properties and the excess energy of the exciting photons. This experiment illustrates a nondestructive way of generating high-pressure tensile waves in strained heterostructures and using them to probe semiconductor structure below the surface of the sample. Since the strength of this nondestructive wave is determined by the strain between GaN and InGaN, it is likely that even stronger coherent phonons can be generated in InGaN/GaN digital alloys grown on a GaN substrate.

II. EXPERIMENTAL RESULTS

In the experiments, frequency-doubled pulses of mode-locked Ti:Sapphire lasers are used to perform reflective pump-probe measurements on four different sample types which are shown in Fig. 1: Type I InGaN epilayers; Type II InGaN/GaN double quantum wells (DQWs); Type III InGaN/GaN single quantum well (SQW); and Type IV InGaN/GaN light-emitting diode (LED) structures. The peak pump power is estimated to be 400 MW/cm^2, corresponding to a carrier density of 10^{19} cm^{-3} and the doubled pulse width is 250 fs. All samples were grown on a c-plane sapphire substrate by metalorganic chemical vapor deposition. The InGaN epilayers shown in Fig. 1(a) consist of 1 μm GaN

 ©2005 The American Physical Society

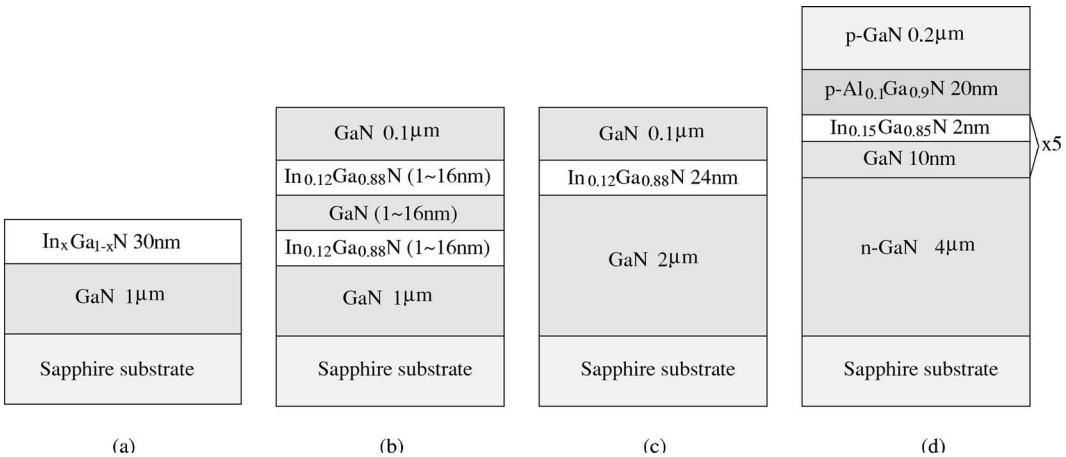

FIG. 1. The simple diagram of the sample structures used in these experiments. (a) InGaN epilayer (Type I), (b) InGaN/GaN DQWs (Type II), (c) GaN SQW (Type III), (d) InGaN/GaN blue LED structure (Type IV).

grown on a sapphire substrate and capped with 30 nm of $In_xGa_{1-x}N$ with In composition, x, varying from 0.04 to 0.12. The DQW sample shown in Fig. 1(b) consists of GaN (1 μm), DQWs of $In_{0.12}Ga_{0.88}N$ (1–16 nm), a barrier of GaN (1–16 nm), and a GaN cap layer (0.1 μm). The SQW sample in Fig. 1(c) consists of GaN (2 μm), an $In_{0.12}Ga_{0.88}N$ well (24 nm), and a GaN cap layer (0.1 μm). The blue LED structure shown in Fig. 1(d) consists of n-GaN (4 μm), five quantum wells of $In_{0.15}Ga_{0.85}N$ (2 nm) and four barriers of GaN (10 nm), p-$Al_{0.1}Ga_{0.9}N$ (20 nm), and p-GaN (0.2 μm).

Differential reflection pump-probe measurements were performed on the $In_xGa_{1-x}N$ epilayers whose structure is shown schematically in Fig. 1(a). Figure 2 shows the oscillatory component of the measured probe differential reflectivity for the InGaN epilayers (Type I) with various In concentrations, x. For comparison purposes, we performed differential reflectivity measurements on a pure GaN HVPE grown sample in order to show that no differential reflectivity oscillations are present in the absence of strain and an epilayer. The energy of the pump laser was varied between 3.22 and 3.35 eV, to keep the excess carrier energy above the InGaN band gap but below the GaN band gap. We note that if the laser energy was below the InGaN band gap, no signal was detected. *Therefore, carrier generation is essential to observing the oscillations*. This is in contrast to a recent coherent optical phonon experiment[12] in which coherent optical phonons in bulk GaN are excited by photons with energies far below the band gap via impulsive stimulated Raman scattering. The inset shows the pump-probe signal prior to the background subtraction for $x=0.12$. The background results from the relaxation of the photoexcited electrons and holes. The oscillations are quite large, on the order of 10^{-2}–10^{-3} and the period is 8–9 ps, *independent* of the In composition but *dependent* on the probe photon energy. The amplitude of the oscillation is approximately proportional to the In concentration indicating that the strain at the InGaN/GaN interface is important. The observed period is approximately $\tau = \lambda/2C_sn$,[13] where λ is the probe beam wavelength, $C_s = 7857$ m/s is the longitudinal acoustic sound velocity in wurtzite GaN, and $n=2.4$ is the refractive index.

We performed two-color pump-probe experiments for a Type III InGaN SQW sample as shown in Fig. 1(b). Figure 3 shows the differential reflectivity oscillations for different probe energies. Note that the period of the oscillation changes *and is proportional to the probe wavelength*. In addition, the amplitude of the differential reflectivity oscillation decreases as the detuning (with respect to the pump) becomes larger. The inset shows the oscillation amplitude as a function of the probe energy in a logarithmic scale and there is an ~2 order of magnitude decrease in differential reflectivity when the probe energy changes from 3.26 eV to 1.63 eV.

Interestingly, Fig. 4 shows that the amplitude of the oscillatory component of the differential reflectivity is independent of the bias voltage, even though the carrier lifetime changes dramatically with voltage bias. Figure 4 shows the

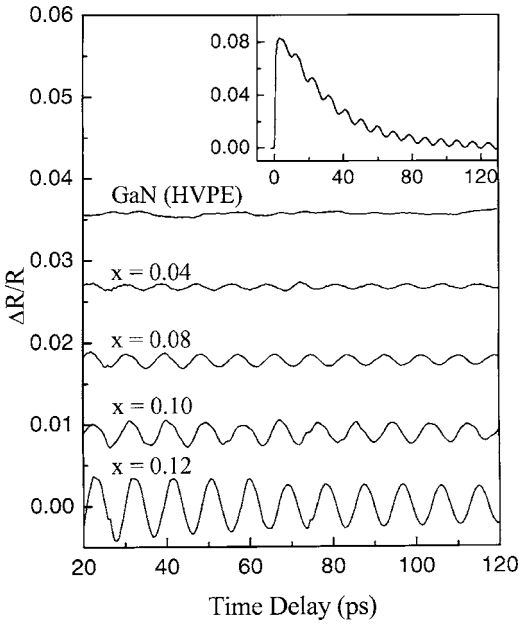

FIG. 2. The oscillatory component of the differential reflection pump-probe data for the $In_xGa_{1-x}N$ epilayers with various In composition ($x=0.04$, 0.08, 0.10, and 0.12). For comparison, differential reflection in a pure GaN high-pressure vapor phase epitaxy (HPVE) grown sample is shown. The reflection signal prior to the background subtraction for $x=0.12$ is shown in the inset.

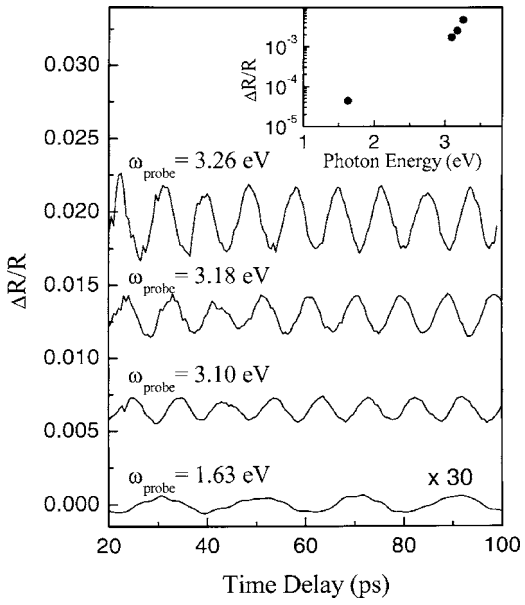

FIG. 3. The oscillation traces of a SQW (III) at different probe energies. The pump energy is centered at 3.26 eV. The bottom curve has been magnified 30 times. The inset shows the oscillation amplitude as a function of probe photon energy on a logarithmic scale.

bias-dependent acoustic phonon differential reflectivity oscillations in a Type IV blue LED structure [see Fig. 1(d)] at a pump energy of 3.17 eV. The lifetime of the background signal drastically decreases as the bias increases as shown in Fig. 4(a). This is due to the carrier recombination time and the decrease in the tunneling escape time in the strong external bias regime.[14] On the other hand, the amplitude and frequency of the oscillatory component of the differential reflectivity does not change much with bias voltage [Fig. 4(b)]. Since the observed reflectivity oscillation is independent of the carrier lifetime for lifetimes as short as 1 ps due to ultrafast tunneling [bottom curve of Fig. 4(a)], it implies that once the source that modulates the experimentally observed

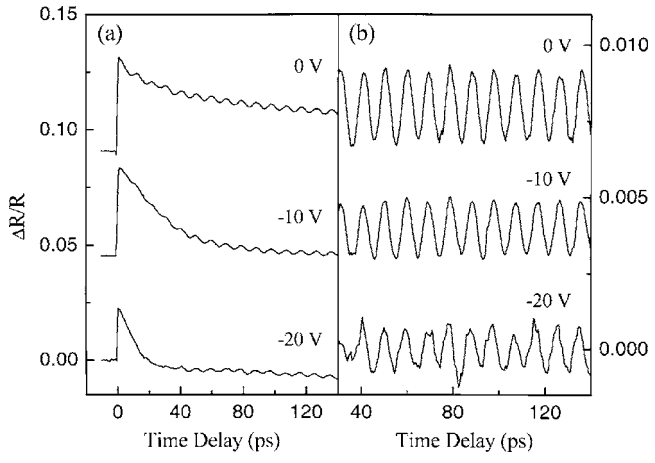

FIG. 4. (a) Pump-probe differential reflectivity for the blue LED structure (Type IV) varying the external bias at a pump energy of 3.17 eV. The decay time of the background signal is drastically reduced as the bias increases. (b) The oscillatory amplitude does not change much with bias.

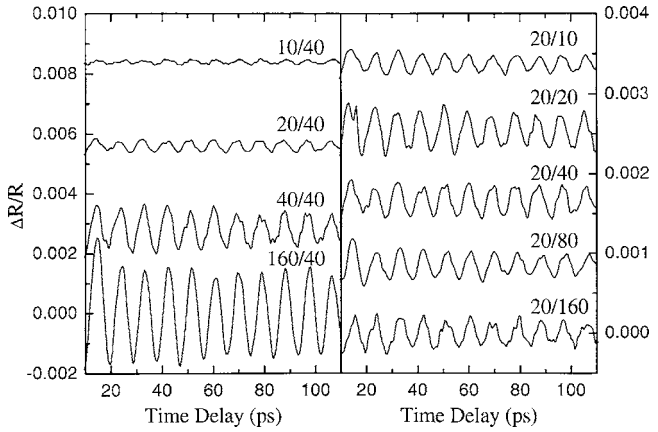

FIG. 5. The oscillatory component of the pump-probe differential transmission traces of DQWs (II) at 3.22 eV. The left figure shows the well width dependence and the right figure shows the barrier width dependence.

reflectivity is launched by the subpicosecond generation of carriers, the remaining carriers do little to affect the source. This suggests that the reflectivity oscillation is due to the strain pulse which is generated at short times once the pump excites the carriers and modulates the lattice constant.

Figure 5 shows the well and barrier-dependent acoustic phonon differential reflectivity oscillations in the Type II DQW samples [see Fig. 1(b)] at a pump energy of 3.22 eV. The amplitude increases as the well width increases. However, the oscillation amplitude of the differential reflectivity does not change much with the barrier width. This means that the generation of the acoustic phonons is due to the InGaN well and not the GaN barrier. This also verifies that the oscillation is due to the strain in InGaN layer.

Interesting results are seen in the long time behavior of the reflectivity oscillations shown in Fig. 6(a). The long-time scale reflectivity oscillation is plotted for the epilayer (I), DQW (II), SQW (III), and the blue LED structure (IV) at 3.29 eV (below the GaN band gap). Astonishingly, the oscillation amplitude abruptly decreases within one cycle of an oscillation at a critical time which appears to scale with the thickness of the GaN layer in each sample. In addition, the slope of the GaN thickness versus the critical time is very close to the known value of the sound velocity in GaN [inset of Fig. 6(a)].[2] Figure 6(b) shows results when the probe laser energy is changed to 3.44 eV which is above the GaN band gap. Then, the laser probe is sensitive to coherent phonon oscillations only within an absorption depth of the surface. We see that the amplitude of the reflectivity oscillation exponentially decays with a decay time of 24.2 ps corresponding to a penetration depth in GaN of about 0.17 micron (=24.2 ps $\times$ 7000 m/s). The oscillation reappears at 260 ps for epilayer (I) and 340 ps for DQW (II). This is twice the critical time for the oscillations to disappear when the photon energy is 3.29 eV. This further shows that the probe pulse is sensitive to the coherent acoustic wave. The "echo" in the probe signal results from the partial reflection of the coherent phonon off the GaN/sapphire interface.

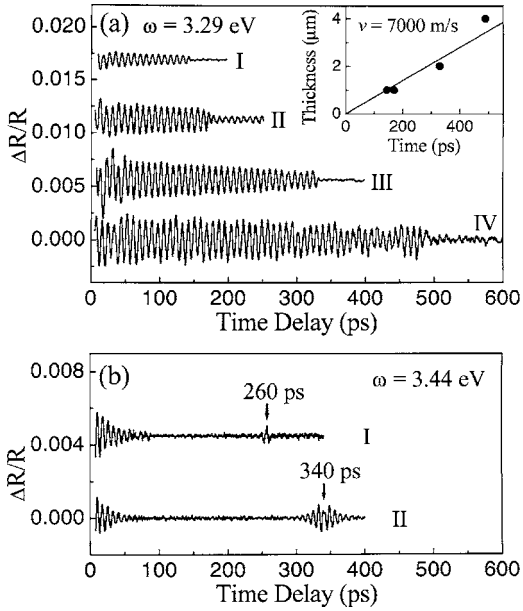

FIG. 6. (a) The long time-scale oscillation traces of an epilayer (I), a DQW (II), a SQW (III), and blue LED structure (IV). The inset shows the GaN thickness between the sapphire substrate and InGaN active layer of the sample as a function of the die out time of the oscillations. The solid line indicates that the velocity of the wave packet in the GaN medium is about 7000 m/s. (b) The oscillation traces of epilayer and DQW [top two curves in (a)] at 3.44 eV which corresponds to a probe laser energy above the band gap of GaN.

III. THEORY

To explain the experimental results discussed in the last section, we have developed a theoretical model of the generation, propagation, and detection of coherent acoustic phonons in strained GaN/InGaN heterostructures. The pump laser pulse generates a strain field that propagates through the sample which, in turn, causes a spatiotemporal change in the index of refraction. This change is responsible for the oscillatory behavior seen in the probe-field reflectivity in various semiconductor heterostructures. An approximate method of solving Maxwell's equations in the presence of spatiotemporal disturbances in the optical properties and obtaining the reflectivity of the probe field in thin films excited by picosecond pump pulses can be found in Thompsen *et al.*[13]

We note that Thompsen *et al.*[13] describes the surface generation and detection of coherent longitudinal optical (LO) phonons due to rapid heating and thermal expansion by a picosecond laser pulse in a-As_2Te_3 and similar compounds. In our experiments, the coherent LO phonon generation mechanism in the strained piezoelectric GaN/InGaN structures has its origin in the deformation and piezoelectric electron-phonon interaction throughout the structure and so the coherent phonon generation mechanisms in the two cases are quite different.

The spatiotemporal disturbance of the refractive index is caused by the propagating coherent phonon wave packets. Thus, an essential ingredient in understanding the probe reflectivity is a model for the generation and propagation of the very short strain pulse in the sample. Recently, a microscopic theory explaining the generation and propagation of such strain pulses was reported by Sanders *et al.* in Ref. 15 (see also the erratum in Ref. 16), where it was shown that propagating coherent acoustic phonon wave packets are created by the nonequilibrium carriers excited by the ultrafast pump pulse. For a tutorial introduction to the generation of coherent acoustic phonons in semiconductor heterostructures, the reader is referred to the recent review article by Chern *et al.*[17] The acoustic phonon oscillations arise through the electron-phonon interaction with the photoexcited carriers. Both acoustic deformation potential and piezoelectric scattering were considered in the microscopic model. It was found that under typical experimental conditions, the microscopic theory could be simplified and mapped onto a loaded string model. Here, we use the string model of coherent phonon pulse generation to obtain the strain field seen by the probe pulse.

First, we solve Maxwell's equations to obtain the probe reflectivity in the presence of a generalized spatiotemporal disturbance of the index of refraction. Let n_b be the index of refraction without the strain which is real because initially the absorption can be neglected and let $\delta\tilde{n}=\delta n+i\kappa$ be the propagating change in the index of refraction due to the strain. When the effect of the change of the index of refraction is taken into account, the probe field with energy ω can be described by the following generalized wave equation

$$\frac{\partial^2 E(z,t)}{\partial z^2}+\frac{\omega^2}{c^2}[n_b+\delta\tilde{n}(z,t)]^2E(z,t)=0, \tag{1}$$

where $E(z,t)$ is the probe field in the slowly varying envelope function approximation and ω is the central frequency of the probe pulse. Equation (1) is obtained from Maxwell's equations assuming that the polarization response is instantaneous and that the probe pulse obeys the slowly varying envelope function approximation. Since $|\delta\tilde{n}|\ll n_b$ under typical conditions, Eq. (1) can be cast into

$$\frac{\partial^2 E(z,t)}{\partial z^2}+(n_bk)^2E(z,t)=-2n_bk^2\delta\tilde{n}(z,t)E(z,t), \tag{2}$$

where $k=\omega/c$ is the probe wave vector.

We view Eq. (2) as an inhomogeneous Helmholtz equation and obtain the solution using the Green's function technique. The desired Green's function is determined by solving

$$\frac{\partial^2 G(z,z')}{\partial z^2}+(n_bk)^2G(z,z')=\delta(z-z'), \tag{3}$$

and the result is

$$G(z,z')=-\frac{i}{2n_bk}\exp(in_bk|z-z'|). \tag{4}$$

Then, the solution to Eq. (2) can be written as

$$E(z,t) = E_h(z,t) + \int_{-\infty}^{\infty} dz' G(z,z')\{-2n_b k^2 \delta\tilde{n}(z',t)E(z',t)\}, \tag{5}$$

$$\approx E_h(z,t) + \int_{-\infty}^{\infty} dz' G(z,z')\{-2n_b k^2 \delta\tilde{n}(z',t)E_h(z',t)\}, \tag{6}$$

where we have chosen the lowest Born series in the last line. In Eq. (6), E_h is the homogeneous solution which takes the form $E_h(z,t)=\tilde{E}_h(z,t)\exp\{i(n_b kz-\omega t)\}$, where $\tilde{E}_h(z,t)$ is a slowly varying envelope function. This describes the probe pulse moving to the right in the sample without optical distortion.

We now apply this approximate solution to our structure where the interface between air and the sample is chosen at $z=0$. In the air, where $z\leqslant 0$, there is an incident probe pulse traveling toward the sample as well as a reflected pulse. The electric field in the air, $E_<(z,t)$, can thus be written as the sum

$$E_<(z,t) = \tilde{E}_{\rm i}(z,t)e^{i(kz-\omega t)} + \tilde{E}_{\rm r}(z,t)e^{-i(kz+\omega t)}, \tag{7}$$

where $\tilde{E}_{\rm i}(z,t)$ and $\tilde{E}_{\rm r}(z,t)$ are the slowly varying envelope functions of the incident and reflected probe fields, respectively. Inside the sample, $z\geqslant 0$, the solution is given as

$$E_>(z,t) = E_h(z,t) + \int_0^{\infty} dz' \exp[in_b k(z'-z)]ik\,\delta\tilde{n}(z',t) \times E_h(z',t)$$

$$\approx \tilde{E}_t(z,t)e^{i(n_b kz-\omega t)} + \left\{\int_0^{\infty} dz' \exp(2in_b kz')ik\,\delta\tilde{n}(z',t)\right\} \times \tilde{E}_t(z,t)e^{-i(n_b kz+\omega t)}, \tag{8}$$

$$= \tilde{E}_t(z,t)e^{i(n_b kz-\omega t)} + \mathcal{A}(n_b k,t)\tilde{E}_t(z,t)e^{-i(n_b kz+\omega t)}, \tag{9}$$

where we used $E_h(z,t)=\tilde{E}_t(z,t)\exp[i(n_b kz-\omega t)]$ in the second step, assuming that $\tilde{E}_t(z,t)$ is nearly constant within the slowly varying envelope function approximation, and we define a reflected amplitude function

$$\mathcal{A}(n_b k,t) \equiv \int_0^{\infty} dz' \exp(2in_b kz')ik\,\delta\tilde{n}(z',t). \tag{10}$$

The expression for the reflected amplitude function, $\mathcal{A}(n_b k,t)$, in Eq. (8) says there is a frequency-dependent modulation of the amplitude in the reflected wave in the sample due to the propagating strain. Let $U(z,t)$ denote the coherent phonon lattice displacement along the [001] growth direction. To relate the change of the index of refraction to the strain field, $\eta(z,t)\equiv \partial U(z,t)/\partial z$, we assume $|\delta\tilde{n}| \ll n_b$ and adopt the linear approximation[13]

$$\delta\tilde{n}(z,t) = \frac{\partial\tilde{n}}{\partial\eta}\eta(z,t). \tag{11}$$

Having determined the waves on both sides of the interface, we can now calculate the reflectivity. We apply the usual boundary conditions to the slowly varying envelope functions and the results are written compactly as

$$\begin{pmatrix} -1 & 1+\mathcal{A} \\ 1 & n_b(1-\mathcal{A}) \end{pmatrix}\begin{pmatrix} \tilde{E}_r \\ \tilde{E}_t \end{pmatrix} = \begin{pmatrix} \tilde{E}_i \\ \tilde{E}_i \end{pmatrix}. \tag{12}$$

We solve this equation to obtain

$$\frac{\tilde{E}_r}{\tilde{E}_i} = \frac{r_0+\mathcal{A}}{1+r_0\mathcal{A}} \approx r_0 + \mathcal{A}, \tag{13}$$

where $r_0=(1-n_b)/(1+n_b)$. To the same order, we find that $\tilde{E}_t/\tilde{E}_i \approx t_0(1-r_0\mathcal{A})$, where $t_0=2/(1+n_b)$. It is now straightforward to calculate the differential reflectivity as

$$\frac{\Delta R}{R} = \frac{|r_0+\Delta r|^2 - |r_0|^2}{|r_0|^2} \approx \frac{2}{r_0}\mathrm{Re}\,\mathcal{A}, \tag{14}$$

where ΔR is the difference in the reflectivity, R, when the pump is on and off, i.e., $\Delta R=R_{\rm on}-R_{\rm off}$. Finally, by substituting the linear law Eq. (11) into Eq. (10) and using Eq. (14), we get

$$\frac{\Delta R}{R} = \int_0^{\infty} dz\ \mathcal{F}(z,\omega)\frac{\partial U(z,t)}{\partial z}, \tag{15}$$

where the sensitivity function, $\mathcal{F}(z,\omega)$, is defined as

$$\mathcal{F}(z,\omega) = -\frac{2k}{r_0}\left[\frac{\partial n}{\partial\eta}\sin(2n_b kz) + \frac{\partial\kappa}{\partial\eta}\cos(2n_b kz)\right]. \tag{16}$$

In Eq. (16) $\partial n/\partial\eta$ and $\partial\kappa/\partial\eta$ are the derivatives with respect to strain of the index of refraction and extinction coefficient, respectively.

In Eq. (15), the differential reflectivity is expressed in terms of the lattice displacement, $U(z,t)$, due to propagating coherent phonons. Sanders *et al.*[15,16] developed a microscopic theory showing that the coherent phonon lattice displacement satisfies a driven string equation,

$$\frac{\partial^2 U(z,t)}{\partial t^2} - C_s^2\frac{\partial^2 U(z,t)}{\partial z^2} = S(z,t), \tag{17}$$

where C_s is the longitudinal acoustic (LA) sound speed in the medium and $S(z,t)$ is a driving term which depends on the photogenerated carrier density. The LA sound speed is related to the mass density, ρ, and the elastic stiffness constant, C_{33}, by $C_s=\sqrt{C_{33}/\rho}$. The LA sound speed is taken to be different in the GaN/InGaN heterostructure and sapphire substrate. For simplicity, we neglect the sound speed mismatch between the GaN and $In_xGa_{1-x}N$ layers.

The driving function, $S(z,t)$, is nonuniform and is given by

$$S(z,t) = \sum_{\nu} S_{\nu}(z,t), \tag{18}$$

where the summation index, ν, runs over carrier species, i.e., conduction electrons, heavy holes, light holes, and crystal-field split holes, that are created by the pump pulse. Each carrier species makes a separate contribution to the driving function. The partial driving functions, $S_{\nu}(z,t)$, in piezoelectric wurtzite crystals depend on the density of the photoexcited carriers. Thus,

$$S_{\nu}(z,t) = \pm \frac{1}{\rho}\left\{ a_{\nu}\frac{\partial}{\partial z} + \frac{4\pi|e|e_{33}}{\epsilon_{\infty}} \right\}\rho_{\nu}(z,t), \tag{19}$$

where the plus sign is used for conduction electrons and the minus sign is used for holes. Here $\rho_{\nu}(z,t)$ is the photogenerated electron or hole number density, which is real and positive, ρ is the mass density, a_{ν} are the deformation potentials for each carrier species, e_{33} is the piezoelectric constant, and ϵ_{∞} is the high-frequency dielectric constant.

To be more specific, we will consider a SQW sample of the type shown in Fig. 1(c). We adopt a simple model for photogeneration of electrons and holes in which the photogenerated electron and hole number densities are proportional to the squared ground state particle in a box wave functions. The exact shape of the electron and hole number density profile is not critical in the present calculation since all that really matters is that the electrons and holes be strongly localized. The carriers are assumed to be instantaneously generated by the pump pulse and are localized in the $In_xGa_{1-x}N$ quantum well. Having obtained a model expression for $\rho_{\nu}(z,t)$, it is straightforward to obtain $S(z,t)$ using Eqs. (18) and (19).

To obtain $U(z,t)$, we solve driven string equations in the GaN epilayer and the sapphire substrate, namely

$$\frac{\partial^2 U(z,t)}{\partial t^2} - C_0^2\frac{\partial^2 U(z,t)}{\partial z^2} = S(z,t) \quad (0 \leqslant z \leqslant L), \tag{20a}$$

and

$$\frac{\partial^2 U(z,t)}{\partial t^2} - C_1^2\frac{\partial^2 U(z,t)}{\partial z^2} = 0 \quad (L \leqslant z \leqslant Z_s), \tag{20b}$$

where C_0 and C_1 are LA sound speeds in the GaN and sapphire substrate, respectively. In Eq. (20b), the sapphire substrate has finite thickness. To simulate coherent phonon propagation in an infinite sapphire substrate, Z_s in Eq. (20b) is chosen large enough so that the propagating sound pulse generated in the GaN epilayer does not have sufficient time to reach $z=Z_s$ during the simulation. If T_{sim} is the duration of the simulation, this implies $Z_s \geqslant L + C_1 T_{\mathrm{sim}}$.

Equations (20a) and (20b) are solved subject to initial and boundary conditions. The initial conditions are

$$U(z,0) = \frac{\partial U(z,0)}{\partial t} = 0. \tag{21}$$

At the GaN-air interface at $z=0$, we assume the free surface boundary condition

$$\frac{\partial U(0,t)}{\partial z} = 0, \tag{22a}$$

since the air exerts no force on the GaN epilayer. The phonon displacement and the force per unit area are continuous at the GaN-sapphire interface so that

$$U(L-\epsilon,t) = U(L+\epsilon,t) \tag{22b}$$

and

$$\rho_0 C_0^2\frac{\partial U(L-\epsilon,t)}{\partial z} = \rho_1 C_1^2\frac{\partial U(L+\epsilon,t)}{\partial z}. \tag{22c}$$

The boundary condition at $z=Z_s$ can be chosen arbitrarily since the propagating sound pulse never reaches this interface. For mathematical convenience, we choose the rigid boundary condition

$$U(Z_s,t) = 0. \tag{22d}$$

To obtain $U(z,t)$ for general $S(z,t)$, we first need to find the harmonic solutions in the absence of strain, i.e., $S(z,t)=0$. The harmonic solutions are taken to be

$$U_n(z,t) = W_n(z)e^{-i\omega_n t} \quad (\omega_n \geqslant 0), \tag{23}$$

and it is easy to show that the mode functions, $W_n(z)$, satisfy

$$\frac{d^2 W_n(z)}{dz^2} + \frac{\omega_n^2}{C_0^2}W_n(z) = 0 \quad (0 \leqslant z \leqslant L), \tag{24a}$$

and

$$\frac{d^2 W_n(z)}{dz^2} + \frac{\omega_n^2}{C_1^2}W_n(z) = 0 \quad (L \leqslant z \leqslant Z_s). \tag{24b}$$

Applying the boundary conditions (22a)–(22d), we obtain the mode functions

$$W_n(z) = \begin{cases} \cos(\omega_n z/C_0) & \text{if } 0 \leqslant z \leqslant L \\ B_n \sin(\omega_n(Z_s - z)/C_1) & \text{if } L \leqslant z \leqslant Z_s \end{cases} \tag{25a}$$

with

$$B_n = \frac{\cos(\omega_n L/C_0)}{\sin(\omega_n(Z_s - L)/C_1)}. \tag{25b}$$

The mode frequencies, ω_n, are solutions of the transcendental equation

$$\frac{1}{\rho_0 C_0}\cot\left(\frac{\omega_n L}{C_0}\right) = \frac{1}{\rho_1 C_1}\tan\left(\frac{\omega_n(Z_s - L)}{C_1}\right), \tag{26}$$

which we solve numerically to obtain the mode frequencies, ω_n $(n=0,1,2,\ldots)$. The index, n, is equal to the number of nodes in the mode functions, $W_n(z)$.

A general displacement can be expanded in terms of the harmonic modes as

$$U(z,t) = \sum_{n=0}^{\infty} q_n(t)W_n(z). \tag{27}$$

Substituting Eq. (27) for $U(z,t)$ into Eqs. (20a) and (20b) and taking the initial conditions (21) into account, we find that

the expansion coefficients, $q_n(t)$, satisfy a driven harmonic oscillator equation

$$\frac{d^2q_n(t)}{dt^2} + \omega_n^2 q_n(t) = Q_n(t), \tag{28}$$

subject to the initial conditions $q_n(0)=dq_n(0)/dt=0$. The harmonic oscillator driving term $Q_n(t)$ is given by

$$Q_n(t) = \frac{\int_0^{Z_s} dz\ W_n(z)S(z,t)}{\int_0^{Z_s} dz\ W_n(z)^2}. \tag{29}$$

In our simple displacive model for photogeneration of carriers, $S(z,t)=S(z)\Theta(t)$, where $\Theta(t)$ is the Heaviside step function. In this case, the lattice displacement is explicitly given by

$$U(z,t) = \sum_{n=0}^{\infty} \frac{S_n}{\omega_n^2}(1-\cos(\omega_n t))W_n(z), \tag{30}$$

with S_n defined as

$$S_n = \frac{\int_0^{Z_s} dz\ W_n(z)S(z)}{\int_0^{Z_s} dz\ W_n(z)^2}. \tag{31}$$

Using the lattice displacement (30), we obtain the time-dependent differential reflectivity at the probe frequency, ω, from Eq. (15). The result is

$$\frac{\Delta R}{R}(\omega,t) = \sum_{n=0}^{\infty} \frac{S_n}{\omega_n^2}(1-\cos(\omega_n t))R_n(\omega), \tag{32}$$

where

$$R_n(\omega) = \int_0^{Z_s} dz\ \mathcal{F}(z,\omega)\frac{dW_n(z)}{dz} \tag{33}$$

can be evaluated analytically.

With the above formalism, we solve for the lattice displacement, $U(z,t)$, for a coherent LA phonon pulse propagating in a multilayer structure consisting of a 1.124 μm thick GaN epilayer grown on top of an infinitely thick sapphire substrate with the growth direction along z. We take the origin to be at the GaN-air interface and the GaN-sapphire interface is taken to be at $z=L=1.124$ μm. We assume that carriers are photogenerated in a single 240 Å thick $In_xGa_{1-x}N$ quantum well embedded in the GaN layer 0.1 μm below the GaN-air interface and 1 μm above the sapphire substrate. Our structure thus resembles the SQW sample shown in Fig. 1(c). In the GaN epilayer, we take $C_{33}=379$ GPa and $\rho_0=6.139$ gm/cm^3 (Ref. 18) from which we obtain $C_0=7857$ m/s. For the sapphire substrate, we take $C_{33}=500$ GPa and $\rho_1=3.986$ gm/cm^3 (Ref. 19) from which we find $C_1=11\,200$ m/s.

The results of our simulation are shown in Fig. 7. A contour map of the strain, $\partial U(z,t)/\partial z$, is shown in Fig. 7(a). We plot the strain as a function of the depth below the surface and the probe delay time. Photoexcitation of electrons and holes in the InGaN quantum well generates two coherent LA sound pulses traveling in opposite directions. The pulses are totally reflected off the GaN/air interface at $z=0$ and are partially reflected at the sapphire substrate at $z=1.124$ μm. Approximately 95% of the pulse energy is transmitted and only 5% is reflected at the substrate. The speed of the LA phonon pulses is just the slope of the propagating wave trains seen in Fig. 7(a), and one can clearly see that the LA sound speed is greater in the sapphire substrate.

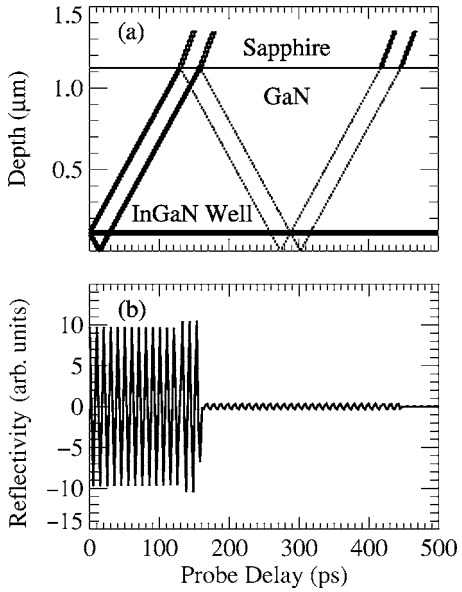

FIG. 7. Generation and propagation of coherent acoustic phonons photogenerated in a single InGaN well embedded in a free standing 1.124 μm GaN epilayer grown on top of a sapphire substrate. In (a), a contour plot of the strain field, $\partial U(z,t)/\partial z$, is shown as a function of depth below the GaN-air interface and the probe delay. In (b), the resulting differential reflectivity induced by the strain field in (a) is shown as a function of the probe delay.

From the strain, the differential reflectivity can be obtained from Eq. (15). From Fig. 7(a), the strains, $\partial U(z,t)/\partial z$, associated with the propagating pulses are highly localized and travel at the LA sound speed. Each pulse contributes a term to the differential reflectivity that goes like

$$\frac{\Delta R}{R}(\omega,t) \sim \mathcal{F}(C_0 t,\omega) \propto \frac{\omega}{c}\sin\left(\frac{2n_b\omega}{c}C_0 t + \phi\right), \tag{34}$$

where the sensitivity function $\mathcal{F}(z,\omega)$ is given in Eq. (16) and ϕ is a phase angle. The period of the oscillations of $\mathcal{F}$ depends on the probe wavelength, $\lambda=2\pi c/\omega$, with the result that the observed differential reflectivity oscillates in time with period, $T=\pi c/(n_b C_0\omega)=\lambda/(2n_b C_0)$, where $n_b=2.4$ is the index of refraction, and $C_0=7857$ m/s is the LA sound speed in GaN. For $\lambda=377$ nm ($\hbar\omega=3.29$ eV), this gives us $T=10$ ps. The sensitivity function, $\mathcal{F}(z,\omega)$, is an oscillating function in the GaN/InGaN epilayer and is assumed to vanish in the sapphire substrate. Our computed differential reflectivity is shown in Fig. 7(b) for a probe wavelength of λ

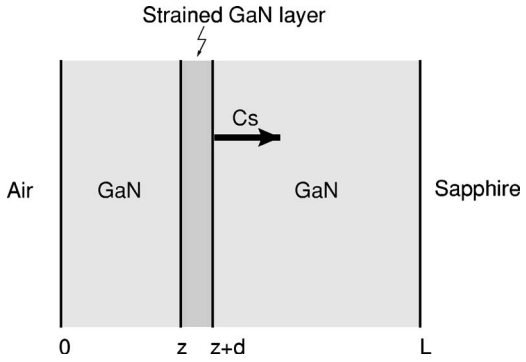

FIG. 8. Propagating strained GaN layer in our simple model. The pump laser pulse creates a coherent acoustic phonon wave packet in the InGaN layer near the air/GaN surface, which is modeled as a thin strained layer. The strained GaN layer propagates into the host GaN layer. The index of refraction in the strained layer is perturbed relative to the background GaN due to the strong strain induced piezoelectric field (Franz-Keldysh effect).

=377 nm. We find that the reflectivity abruptly attenuates when the strain pulse enters the sapphire substrate at t =170 ps. The reflected strain pulses give rise to the weaker oscillations seen for $t>170$ ps. These oscillations are predicted to continue until the reflected pulses are again partially reflected off the sapphire substrate at t=430 ps.

IV. SIMPLE MODEL

Since the coherent oscillation observed in the differential reflectivity stems essentially from the strain pulse propagating into the layers, most phenomena can be understood by a simple macroscopic model that is presented in this section.

Instead of solving the loaded string equations for the strain to obtain a propagating disturbance in the refractive index, the propagating strain pulse at a given moment can be viewed as a thin strained layer in the sample, where the index of refraction is assumed to be slightly different from the rest of the sample. This situation is schematically depicted in Fig. 8 where a fictitious thin GaN strained layer is located at z in the thick host GaN layer. The thickness of the strained layer, d, is approximately the width of the traveling coherent phonon strain field, $\partial U(z,t)/\partial z$, and is to be determined from the microscopic theory. From the last section, it was seen that the propagating strain field is strongly localized so that d is small. In the example of the last section, d is approximately equal to the quantum well width. Here, we assume the strain pulse has been already created near the air/GaN interface and do not consider its generation procedure. We treat d as a phenomenological constant and also assume that the change in the index of refraction is constant. This strained GaN layer travels into the structure with the speed of the acoustic phonon wave packet $C_0=7\times10^3$ m/s, so the location of the stained layer is given as $z=C_0\tau$ where τ is the pump-probe delay time.

Within the slowly varying envelope function approximation, the solutions to the Maxwell equation can be written as plane waves in each region,

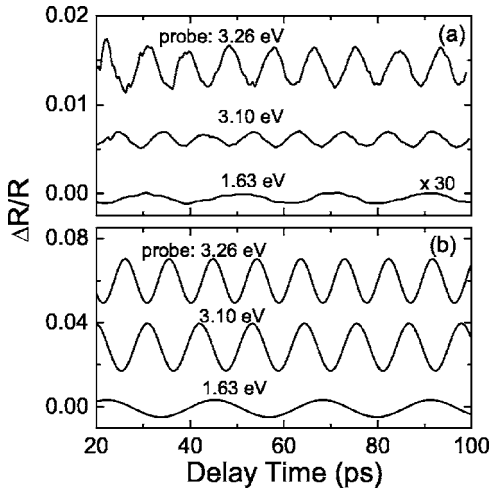

FIG. 9. Differential reflection for different frequencies of the probe pulse. Plot (a) is experimental data and (b) comes from our calculations.

$$E_i(z,t) = a_i e^{ik_i z_i - i\omega t} + b_i e^{-ik_i z_i - i\omega t}, \tag{35}$$

where E_i is the electric field in the left layer of ith interface, and a_i and b_i are the slowly varying amplitudes. The magnetic field is given by $B_i \sim \partial E_i/\partial z$. For a normally incident probe field, we apply the usual matching conditions on E and B to obtain

$$\begin{pmatrix} a_i \\ b_i \end{pmatrix} = \mathcal{M}_i \begin{pmatrix} a_{i+1} \\ b_{i+1} \end{pmatrix}, \tag{36}$$

where the transfer matrix, $\mathcal{M}_i$, is given explicitly as

$$\mathcal{M}_i = \frac{1}{2}\begin{pmatrix} \left(1+\frac{k_{i+1}}{k_i}\right)e^{i(k_{i+1}-k_i)z_i} & \left(1-\frac{k_{i+1}}{k_i}\right)e^{-i(k_{i+1}+k_i)z_i} \\ \left(1-\frac{k_{i+1}}{k_i}\right)e^{i(k_{i+1}+k_i)z_i} & \left(1+\frac{k_{i+1}}{k_i}\right)e^{-i(k_{i+1}-k_i)z_i} \end{pmatrix}. \tag{37}$$

To apply this formula to our configuration, we normalize the incident amplitude to 1, let r be the reflected amplitude in the air, and impose the boundary condition that there is only a transmitted wave into the sapphire substrate with amplitude t and no reflected wave from the GaN-sapphire interface back into the GaN epilayer. The latter assumption is reasonable since the microscopic theory of the previous section shows that only 5% of the pulse energy is reflected from the interface between the GaN and the sapphire substrate. The total reflection and transmission amplitudes r and t for the GaN epilayer structure are determined by

$$\begin{pmatrix} 1 \\ r \end{pmatrix} = \begin{pmatrix} \mathcal{M}_{11} & \mathcal{M}_{12} \\ \mathcal{M}_{21} & \mathcal{M}_{22} \end{pmatrix}\begin{pmatrix} t \\ 0 \end{pmatrix}, \tag{38}$$

where $\mathcal{M}=\mathcal{M}_1\mathcal{M}_2\cdots\mathcal{M}_n$. The reflection amplitude is readily found to be

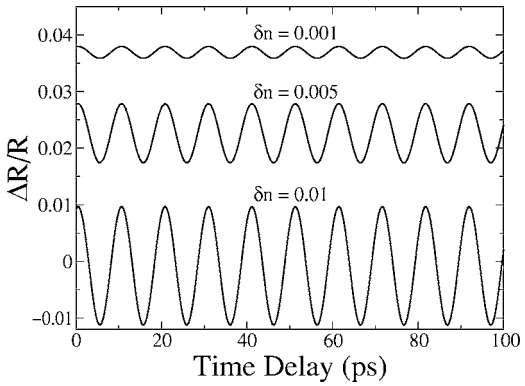

FIG. 10. The differential reflection calculated numerically using Eq. (14) for three different values in the change in index of refraction. The parameters used are $n_b=2.65$, $\omega=3.29$ eV, $d=30$ nm, $L=1$ μm, and $C_s=7000$ m/s. (Note that the curves are sifted to avoid overlapping.)

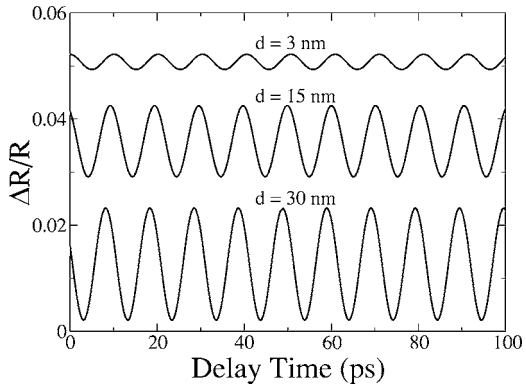

FIG. 11. Calculated differential reflection for different values of the thickness of the strained GaN layer. The parameters are $n_b=2.65$, $\omega=3.29$ eV, $L=1$ μm, and $C_s=7000$ m/s. The change in the index of refraction in the strained GaN layer was assumed to be $\delta n=0.01$.

$$r=\mathcal{M}_{21}/\mathcal{M}_{11}=r_0+\Delta r, \tag{39}$$

where r_0 is the background contribution without the strained layer. The total transmission amplitude is given as $t=1/\mathcal{M}_{11}$. We can now numerically calculate the differential reflectivity by substituting r into Eq. (14).

In Fig. 9, we compare our theoretical model with experimental results. In Fig. 9(a), the oscillatory part of the differential reflectivity is plotted as a function of probe delay for three values of the probe photon energy. These are the same data that were shown in Fig. 3 where it was seen that the oscillation period of the coherent phonon reflectivity oscillations are proportional to the probe wavelength. In Fig. 9(b), we plot the corresponding theoretical differential reflectivities obtained from Eq. (14). Comparing Figs. 9(a) and 9(b), we see that our geometrical optics model successfully explains the observed relation between the coherent phonon oscillation period and the probe wavelength. However, the calculated amplitudes of oscillation are inconsistent with the experimental data because, in this case, we have not taken into account the change of index of refraction with respect to the probe wavelength, which we will do later in the paper.

In Fig. 10, we plot the differential reflectivity as a function of the probe delay for three different values of the change in the index of refraction in the strained layer, $\delta\tilde{n}$. As expected, the greater the change in index of refraction, the greater the amplitude of the differential reflectivity oscillations. A larger change in the index of refraction implies that more electron-hole pairs are excited near the air-GaN interface, which acts as a stronger source for the coherent acoustic phonon reflectivity oscillations. These results are qualitatively consistent with the experimental results shown in Fig. 2. In Fig. 11, we fix the change in the index of refraction, $\delta n=0.01$, and varied the thickness of the strained layer, d. The result shows a larger amplitude for the differential reflection in wider strained layers, which is consistent with what was experimentally observed in Fig. 5.

Both Figs. 10 and 11 suggest that the amplitude of the differential reflectivity seems to increase monotonically with δn and d. All of these features can be understood more easily using the single-reflection approximation to the full formula for the reflectivity in Eq. (39). Assuming the change in the index of refraction is small, $|\delta\tilde{n}|\ll 1$, we may select contributions from only terms proportional to $\delta\tilde{n}$ in the infinite Fabry-Perot series for the total reflection amplitude. The relevant reflection processes selected are schematically depicted in Fig. 12. In this case, the total reflection amplitude is given by the leading terms in the Fabry-Perot series

$$r=r_0+r_1+r_2+\mathcal{O}(\delta\tilde{n}^2), \tag{40}$$

where r_0 is the background reflection amplitude, and the first-order terms in $\delta\tilde{n}$ are

$$r_1\propto -e^{2ikz}\delta\tilde{n}, \quad r_2\propto e^{i2k(z+d)}\delta\tilde{n}. \tag{41}$$

To linear order in $\delta\tilde{n}$, the differential reflectivity Eq. (14) becomes

$$\frac{\Delta R}{R}=\frac{8\sin(kd)}{n^2-1}[\delta n\sin(2kz+kd)+\kappa\cos(2kz+kd)]$$
$$=\frac{8\sin(kd)}{n^2-1}|\delta\tilde{n}|\sin(kd)\sin(2kz+\phi), \tag{42}$$

where the phase ϕ is given by

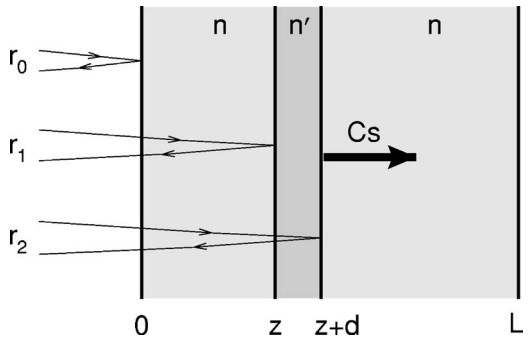

FIG. 12. Schematic diagram of the single-reflection approximation in the Fabry-Perot reflection; where we have selected the processes only proportional to $\delta\tilde{n}$ $(=n'-n)$.

$$\phi = kd + \arctan\left(\frac{\kappa}{\delta n}\right). \tag{43}$$

Note that for small values of kd, we can expand Eq. (42) in a Taylor series to obtain

$$\frac{\Delta R}{R} = \frac{8kd}{n^2 - 1}[\delta n \sin(2kz) + \kappa \cos(2kz)] \tag{44}$$

to first order in kd.

From Eq. (42), one can see that the amplitude of the oscillation scales linearly with the change in the real part and imaginary part of the index of refraction, respectively.

Since the strain-pulse front moves with the speed of sound, $z = C_0 t$, one can rewrite Eq. (42) as

$$\frac{\Delta R}{R}(\omega, t) \propto |\delta\tilde{n}| \sin(kd) \sin\left(2\pi\frac{t}{T} + \phi\right), \tag{45}$$

where $T = \pi c/(n_b C_0 \omega) = \lambda/(2C_0 n_b)$. Note that in the long-wavelength limit, $kd \to 0$, Eq. (45) is equivalent to Eq. (34) of the microscopic theory described in the last section.

Equation (45) shows that the period of oscillations in the differential reflectivity is given by T and hence is determined by the wavelength of the probe pulse. This is consistent with what was seen in these experiments, but differs from previous experiments where the frequency of coherent phonon oscillation was determined by the sample and not the external probe. Note also that Eq. (45) explains the experimental dependence of the amplitude of the oscillation. It is proportional to the change in the index of refraction and varies with $\sin(kd)$, and hence will increase linearly with the thickness of the strained layer as well as the probe frequency ω for $kd = n_b(\omega/c)d \ll 1$.

Finally, we would like to mention the possibility of using multiple pump pulses to coherently control the generated coherent phonons in the epilayers. There have already been quite a few coherent control experiments with multiple quantum wells from several different groups, such as Sun,[20] Özgür,[21] and Nelson.[22] In the InGaN/GaN epilayer systems, the effect of multiple pump pulses should be more prominent than in AlGaAs/GaAs systems because of the stronger piezoelectric field. This might lead to novel applications in imaging, or possibly new devices based on coherent acoustic phonons.

V. CONCLUSION

We have presented a theory for the detection of a new class of large amplitude coherent acoustic phonon wave packets in femtosecond pump-probe experiments on $In_xGa_{1-x}N/GaN$ epilayers and heterostructures. The InGaN/GaN structures are highly strained, and at high In concentrations have large built-in piezoelectric fields which account for the large amplitude of the observed reflectivity oscillations. This new class of coherent acoustic phonons is generated near the surface and propagates into the structure. The frequency of the reflectivity oscillations is found to be proportional to the frequency of the probe. These coherent phonon wave packets can be used as a powerful probe of the structure of the sample. We are able to model the generation and propagation of these acoustic phonon wave packets using a simple string model which is derived from a microscopic model for the photogeneration and propagation of coherent acoustic phonon wave packets in InGaN/GaN multiple quantum wells. Our model successfully predicts the observed dependence of the coherent phonon reflectivity oscillations on probe wavelength and epilayer thickness.

ACKNOWLEDGMENTS

This work was supported by the National Science Foundation through Grant No. DMR 9817828 and the Department of Energy through Grant No. DE-FG02-02ER45984. One of us (C.S.K.) acknowledges support from the Korea Research Foundation and KOSEF through Grant No. R05-2003-000-11432-0. We gratefully acknowledge useful discussions with Chi-Kuang Sun.

[1] S. Nakamura, S. Pearton, and G. Fasol, *The Blue Laser Diode: The Complete Story* (Springer, Berlin, 2000).
[2] C. K. Sun, J. C. Liang, and X. Y. Yu, Phys. Rev. Lett. **84**, 179 (2000).
[3] Ü. Özgür, C. W. Lee, and H. O. Everitt, Phys. Status Solidi B **228**, 85 (2001).
[4] A. Yamamoto, T. Mishina, Y. Masumoto, and M. Nakayama, Phys. Rev. Lett. **73**, 740 (1994).
[5] A. Bartels, T. Dekorsy, H. Kurz, and K. Köhler, Phys. Rev. Lett. **82**, 1044 (1999).
[6] K. Mizoguchi, M. Hase, S. Nakashima, and M. Nakayama, Phys. Rev. B **60**, 8262 (1999).
[7] P. Lefebvre, A. Morel, M. Gallart, T. Taliercio, J. Allègre, B. Gil, H. Mathieu, B. Damilano, N. Grandjean, and J. Massies, Appl. Phys. Lett. **78**, 1252 (2001).
[8] T. Takeuchi, C. Wetzel, S. Yamaguchi, H. Sakai, H. Amano, I. Akasaki, Y. Kaneko, S. Nakagawa, Y. Yamaoka, and N. Yamada, Appl. Phys. Lett. **73**, 1691 (1998).
[9] J. S. Im, H. Kollmer, J. Off, A. Sohmer, F. Scholz, and A. Hangleiter, Phys. Rev. B **57**, R9435 (1998).
[10] S. F. Chichibu, A. C. Abare, M. S. Minsky, S. Keller, S. B. Fleischer, J. E. Bowers, E. Hu, U. K. Mishra, L. A. Coldren, S. P. DenBaars *et al.*, Appl. Phys. Lett. **73**, 2006 (1998).
[11] J. S. Yahng, Y. D. Jho, K. J. Yee, E. Oh, J. C. Woo, D. S. Kim, G. D. Sanders, and C. J. Stanton, Appl. Phys. Lett. **80**, 4723 (2002).
[12] K. J. Yee, K. G. Lee, E. Oh, D. S. Kim, and Y. S. Lim, Phys. Rev. Lett. **88**, 105501 (2002).
[13] C. Thomsen, H. T. Grahn, H. J. Maris, and J. Tauc, Phys. Rev. B **34**, 4129 (1986).
[14] Y. D. Jho, J. S. Yahng, E. Oh, and D. S. Kim, Appl. Phys. Lett. **79**, 1130 (2001).

[15] G. D. Sanders, C. J. Stanton, and C. S. Kim, Phys. Rev. B **64**, 235316 (2001).
[16] G. D. Sanders, C. J. Stanton, and C. S. Kim, Phys. Rev. B **66**, 079903(E) (2002).
[17] C. W. Chern, C. K. Sun, G. D. Sanders, and C. J. Stanton, in *Ultrafast Dynamical Processes in Semiconductors*, edited by K. T. Tsen (Springer, New York, 2004), pp. 339–394.
[18] O. Ambacher, J. Smart, J. R. Shealy, N. G. Weimann, K. Chu, M. Murphy, W. J. Schaff, L. F. Eastman, R. Dimitrov, L. Wittmer *et al.*, J. Appl. Phys. **85**, 3222 (1999).
[19] A. G. Every, G. L. Koos, and J. P. Wolfe, Phys. Rev. B **29**, 2190 (1984).
[20] C. K. Sun, Y. K. Huang, J. C. Liang, A. Abare, and S. P. DenBaars, Appl. Phys. Lett. **78**, 1201 (2001).
[21] Ü. Özgür, C. W. Lee, and H. O. Everitt, Phys. Rev. Lett. **86**, 5604 (2001).
[22] T. Feurer, J. C. Vaughan, and K. A. Nelson, Science **299**, 374 (2003).